Synthesis of Cobalt Oxide Nanotubes from Colloidal Particles Modified with a Co(III)−Cysteinato Precursor

Xiangyang Shi, Shubo Han, Raymond J. Sanedrin, Feimeng Zhou,* and Matthias Selke*

Department of Chemistry and Biochemistry, California State University, Los Angeles, Los Angeles, California 90032

Received December 11, 2001. Revised Manuscript Received February 21, 2002

The fabrication of cobalt oxide nanotubes (length 3−4 μm, width 200−400 nm) was achieved by a colloidal templating approach. In this approach, a Co(III)−cysteinato complex $[Co(en)_2(S\text{-}cys)]^{2+}2(BF_4^-)$ was employed as the precursor of cobalt oxide. The infiltration behavior of the precursor into polyelectrolyte multilayers was studied with a quartz crystal microbalance which showed that the amount of the precursor incorporated increased with the number of polyelectrolyte (PE) layers. After incorporation of the precursor into PE multilayers precoated onto submicron-sized polystyrene latex particles via the layer-by-layer deposition, the resulting composite colloidal particles became threaded in a pearl necklace-like structure. Upon calcination at an elevated temperature, cobalt oxide nanotubes were observed by transmission electronic microscopy (TEM) and atomic force microscopy. High-resolution TEM, electron diffraction, energy-dispersive X-ray spectroscopy, and X-ray diffraction showed that these nanotubes were composed of spinel polycrystalline Co_3O_4. The preparation of such cobalt oxide nanotubes affords a new avenue for the application of metal complexes and represents a promising route for the synthesis of novel inorganic nanotubes.

Introduction

Nanotubes represent a new special form of materials, and their unique properties may find a wide range of potential applications in catalysis, sensing, tribology, and electronic nanodevices.[1−4] Since the discovery of multiwalled[5] and single-walled[6−8] carbon nanotubes, exploration of the potential applications of various inorganic and organic nanotubes has engendered a great deal of interest. Much attention has also been directed to the fabrication of inorganic nanotubes.[9,10] A myriad of inorganic nanotubes (e.g., WS_2,[9] MoS_2,[11] V_2O_5,[12] and silica[13]) have been constructed using various chemical or physical methods, such as high-temperature heating in a controlled atmosphere,[11] arc discharge,[14] sol−gel,[12,13,15] electrosynthesis,[16,17] templating,[18−20] and chemical or surfactant-assisted processing.[21−24]

Cobalt oxide-based materials are suitable candidates for the construction of solid-state sensors,[25,26] heterogeneous catalysts,[27,28] electrochromic devices,[29] and solar energy absorbers.[30,31] To our knowledge, there are few reports about the production of cobalt oxide nano-

* To whom correspondence should be addressed. F. Zhou: e-mail fzhou@calstatela.edu; phone 323 343 2390; Fax 323 343 6490. M. Selke: e-mail mselke@calstatela.edu.

(1) Martin, C. R. *Acc. Chem. Res.* **1995**, *28*, 61.
(2) Hu, J. T.; Odom, T. W.; Lieber, C. M.; L. *Acc. Chem. Res.* **1999**, *32*, 435−445.
(3) Rao, C. N. R.; Satishkumar, B. C.; Govindaraj, A.; Nath, M. *Chemphyschem* **2001**, *2*, 78−105.
(4) Park, H.; Park, J.; Lim, A. K. L.; Anderson, E. H.; Alivisatos, A. P.; McEuen, P. L. *Nature (London)* **2000**, *407*, 57−60.
(5) Iijima, S. *Nature (London)* **1991**, *354*, 56−58.
(6) Iijima, S.; Ichihashi, T. *Nature (London)* **1993**, *363*, 603−605.
(7) Bethune, D. S.; Kiang, C. H.; deVries, M. S.; Gorman, G.; Savoy, R.; Vazquez, J.; Beyers, R. *Nature (London)* **1993**, *363*, 605−607.
(8) O'Loughlin, J. L.; Kiang, C. H.; Wallace, C. H.; Reynolds, T. K.; Rao, L.; Kaner, R. B. *J. Phys. Chem. B* **2001**, *105*, 1921−1924.
(9) Tenne, R.; Margulis, L.; Genut, M.; Hodes, G. *Nature (London)* **1992**, *360*, 444−446.
(10) Tremel, W. *Angew. Chem., Int. Ed.* **1999**, *38*, 2175−2179.
(11) Feldman, Y.; Wasserman, E.; Srolovitz, D. J.; Tenne, R. *Science* **1995**, *267*, 222−225.
(12) Krumeich, F.; Muhr, H. J.; Niederberger, M.; Bieri, F.; Schnyder, B.; Nesper, R. *J. Am. Chem. Soc.* **1999**, *121*, 8324−8331.
(13) Nakamura, H.; Matsui, Y. *J. Am. Chem. Soc.* **1995**, *117*, 2651−2652.
(14) Loiseau, A.; Willame, F.; Demoncy, N.; Hug, H.; Pascard, H. *Phys. Rev. Lett.* **1996**, *76*, 4737−4740.
(15) Lakshmi, B. B.; Patrissi, C. J.; Martin, C. R. *Chem. Mater.* **1997**, *9*, 2544−2550.
(16) Pu, L.; Bao, X.; Zou, J.; Feng, D. *Angew. Chem., Int. Ed.* **2001**, *40*, 1490−1493.
(17) Chopra, N. G.; Luyken, R. J.; Cherry, K.; Crespi, V. H.; Cohen, M. L.; Louie, S. G.; Zettl, A. *Science* **1995**, *269*, 966.
(18) Martin, C. R. *Science* **1994**, *266*, 1961.
(19) Sapp, S. A.; Lakshmi, B. B.; Martin, C. R. *Adv. Mater.* **1999**, *11*, 402−404.
(20) Shenton, W.; Douglas, T.; Young, M.; Stubbs, G.; Mann, S. *Adv. Mater.* **1999**, *11*, 253.
(21) Schaak, R. E.; Mallouk, T. E. *Chem. Mater.* **2000**, *12*, 3427−3434.
(22) Saupe, G. B.; Waraksa, C. C.; Kim, H. N.; Han, Y. J.; Kaschak, D. M.; Skinner, D. M.; Mallouk, T. E. *Chem. Mater.* **2000**, *12*, 1556−1562.
(23) Kasuga, T.; Hiramatsu, M.; Hoson, A.; Sekino, T.; Niihara, K. *Adv. Mater.* **1999**, *11*, 1307.
(24) Li, Y.; Wang, J.; Deng, Z.; Wu, Y.; Sun, X.; Yu, D.; Yang, P. *J. Am. Chem. Soc.* **2001**, *123*, 9904−9905.
(25) Yamaura, H.; Tamaki, J.; Moriya, K.; Miura, N.; Yamazoe, N. *J. Electrochem. Soc.* **1997**, *144*, L158.
(26) Ando, M.; Kobayashi, T.; Lijima, S.; Haruta, M. *J. Mater. Chem.* **1997**, *7*, 1779−1783.
(27) Nkeng, P.; Koening, J.; Gautier, J.; Chartier, P.; Poillerat, G. *J. Electroanal. Chem.* **1996**, *402*, 81.
(28) Weichel, S.; Moller, P. J. *Surf. Sci.* **1998**, *399*, 219.
(29) Burke, L. D.; Lyons, M. E.; Murphy, O. J. *J. Electroanal. Chem.* **1982**, *132*, 247.
(30) Hutchins, M. G.; Wright, P. J.; Grebenik, P. D. *Solar Energy Mater.* **1987**, *16*, 113.
(31) Ramachandram, K.; Oriakhi, C. O.; Lerner, M. M.; Koch, V. R. *Mater. Res. Bull.* **1996**, *31*, 767.

10.1021/cm011630i CCC: $22.00
Published on Web 03/27/2002

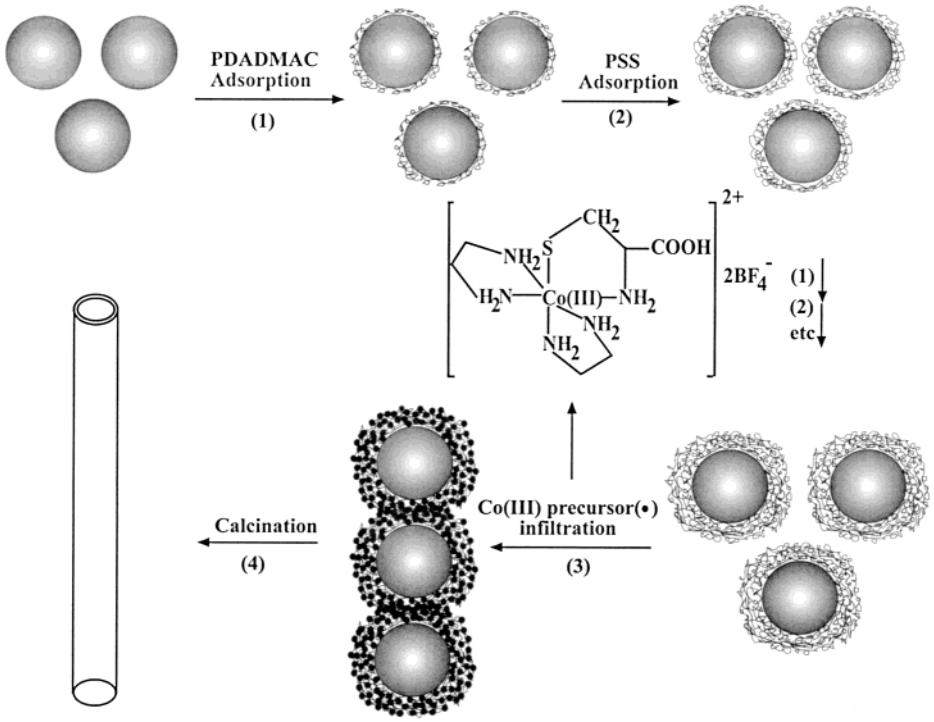

Figure 1. Schematic representation of the experimental procedure for the fabrication of cobalt oxide nanotubes. The structure of the precursor is also given.

tubes. The major example that we are aware of is the cobalt oxide nanofibers prepared by Martin and co-workers using the sol−gel method combined with a membrane-based synthesis.[15]

In this paper, we report the construction of cobalt oxide nanotubes by a colloidal templating method originally developed by Caruso and co-workers for the fabrication of inorganic hollow spheres[32,33] and planar films.[34] We found that the Co(III)−cysteinato complex, $[Co(en)_2(S\text{-}cys)]^{2+}([BF_4]^-)2$ (Co-S-cys),[35,36] whose structure is shown in Figure 1, can easily be incorporated into polyelectrolyte (PE) multilayers predeposited onto colloidal particles and become the precursor for the formation of cobalt oxide nanotubes. Adsorption of PE multilayers onto colloidal particles was verified by transmission electron microscopy (TEM), and the incorporation of Co-S-cys into PE multilayer-coated particles was investigated using a quartz crystal microbalance (QCM). The chemical composition and crystalline phases of the observed nanotubes were investigated with electron diffraction, X-ray diffraction (XRD), and energy-dispersive X-ray spectroscopy (EDX), while the dimension and structure were measured with TEM and atomic force microscopy (AFM).

Previous attempts[32,33] of incorporating precursors into the PE coatings of colloidal particles (e.g., utilizing the incorporation of titanium(IV) bis(ammonium lactato)-dihydroxide (TALH) as a precursor into the PE-coated nanospheres[32]) resulted in the exclusive formation of intact or broken hollow spheres upon thermal treatment. Therefore, the formation of cobalt-containing nanotubes (instead of cobalt-containing hollow spheres) is quite unexpected. We ascribe the formation of the cobalt-containing nanotubes to the unique chemical structure of the precursor. Through the systematic characterization of the resultant materials, we are able to demonstrate that shapes of exotic metal-containing nanomaterials are related not only to the preparative method but also to the chemical nature of the precursor.

Experimental Section

Materials. Negatively charged, sulfate stabilized polystyrene (PS) particles (diameter = 600 nm) were acquired from Interfacial Dynamics Corp. (Portland, OR). Poly(diallyldimethylammonium chloride) (PDADMAC), M_w = 200 000−350 000, and poly(sodium 4-styrenesulfonate) (PSS), M_w = 70 000, were purchased from Aldrich. The cobalt(III)−cysteinato precursor $[Co(en)_2(S\text{-}cys)]^{2+}([BF_4]^-)2$ (Co-S-cys) was synthesized and characterized by NMR and UV/vis using procedures described in the literature.[35,36] All polyelectrolytes were used as aqueous solutions at a concentration of 1 mg/mL (containing 0.5 M NaCl). The Co-S-cys precursor was dissolved in water with a concentration of 30 mg/mL at neutral pH. Water used in all experiments was purified with a three-stage Millipore Milli-Q Plus 185 system and had a resistivity higher than 18.2 MΩ cm.

Infiltration of Co-S-cys into PE Multilayers. Thin, alternating PDADMAC/PSS multilayer films were assembled onto an AT-cut 9.995 MHz gold-coated quartz crystal (ICM Technologies, Oklahoma City, OK) via the layer-by-layer (LbL) method. Before the PE multilayer assembling, the QCM crystal surface was cleaned with a piranha solution (30% H_2O_2 and 70% concentrated H_2SO_4). *CAUTION*: *Piranha solution reacts violently with organic solvents and is a skin irritant. Extreme caution should be exercised when handling piranha solution.* After thoroughly washing with water, the crystal was dried under a gentle N_2 stream. This step was followed by immersing the crystal in a PDADMAC solution for 15 min, rinsing the excess PE off the crystal by dipping in water for 1 min for three

(32) Caruso, F.; Shi, X.; Caruso, R. A.; Susha, A. *Adv. Mater.* **2001**, *13*, 740−744.
(33) Wang, D. Y.; Caruso, R. A.; Caruso, F. *Chem. Mater.* **2001**, *13*, 364−371.
(34) Shi, X.; Cassagneau, T.; Caruso, F. *Langmuir* **2002**, *18*, 904−910.
(35) Galvez, C.; Ho, D. G.; Azod, A.; Selke, M. *J. Am. Chem. Soc.* **2001**, *123*, 3381−3382.
(36) Sloan, C. P.; Krueger, J. H. *Inorg. Chem.* **1975**, *14*, 1481.

times, and drying with a gentle stream of N_2. PSS was then adsorbed onto the PDADMAC-modified quartz crystal for 15 min. This was again followed by rinsing and drying. PDADMAC/PSS films with a desired layer number were fabricated by repetitive alternate deposition of PDADMAC and PSS. Infiltration of the Co-S-cys precursor was accomplished by exposing the multilayered PE films to a Co-S-cys solution (30 mg/mL) for 30 min. The number of PE layers was varied in order to study the dependence of the amount of infiltrated precursor on the thickness of the PE multilayers.

Frequency measurements were carried out before and after the Co-S-cys infiltration through the use of an ICM oscillator and a PM6680B counter/timer (Fluke Corp., Everett, WA). The total mass deposited onto the QCM crystal surface can be calculated from the cumulative frequency change using the Sauerbrey equation.[37] For a 9.995 MHz QCM crystal with an electrode area of 0.196 cm^2, the relationship between the adsorbed mass (Δm) of Co-S-cys and the change in the resonant frequency (ΔF) is given by

$$\Delta m \text{ (ng)} = -0.86\Delta F \text{ (Hz)} \quad (1)$$

Preparation of Cobalt Oxide Nanotubes. 50 μL of a concentrated suspension of PS spheres (5.8 wt % solution) was diluted to 1 mL with water. After dispersion, 1 mL of a PDADMAC solution was added and well mixed. Upon a 15 min PDADMAC adsorption, the excess PDADMAC was removed by three repeated centrifugation (3800*g*, 10 min) and washing cycles. The subsequent steps for forming the alternate PE multilayers and for incorporating the Co-S-cys precursor followed the aforementioned procedure except that the Co-S-cys precursor adsorption time was 30 min. In all cases, the PE concentrations were sufficient to yield a full PE surface coverage onto the nanosphere surface or the preceding PE layers.[38] Cobalt oxide nanotubes were produced by air-drying the coated PS spheres on quartz slides at room temperature, followed by calcining (heating rate = 5 °C min^{-1}) at 385 °C under N_2 and O_2 for 2 and 6 h, respectively.

Instrumentation. The incorporation of the Co-S-cys precursor onto the PS particles was determined by FTIR (NEXUS 870, Nicolet Instruments, Madison, WI). Spectra of dried powders of Co-S-cys, PS particles coated with 10 PE layers (designated as PS + PE10), and PS particles covered with the PE layers containing the precursor (PS + PE10 + Co-S-cys) were all measured. TEM were performed on a JEOL 1200 CX2 microscope operated at 120 kV. A JEOL JEM-2000 FX microscope that is capable of determining the electron diffraction pattern was used to obtain the high-resolution TEM (HRTEM) images at 200 kV. Scanning electron microscope (SEM) measurements were carried out with a Cambridge Stereoscan 250 instrument at 20 kV that is equipped with a Link energy-dispersive X-ray analyzer. SEM samples (on silicon substrates) were sputtered with about 5 nm Au. AFM measurements were conducted using an AFM equipped with a magnetic alternating current (MAC) mode (Molecular Imaging, Phoenix, AZ). Both contact and MAC modes were employed for the characterization of cobalt oxide nanotubes. The MAC cantilever tips used had a spring constant of 0.5 N/m. Images of cobalt oxide nanotubes on silicon wafers were obtained using an oscillating frequency of 25 kHz and a driver current of 30 ± 5 A. The amplitude change of the probe was sufficiently low, and consequently the imaging was nondestructive to the samples. XRD measurements were performed using a Rigaku X-ray diffractometer (Cu Kα radiation, 50 kV, 70 mA). PS particles coated with the PE/precursor films were put down onto silicon wafers, air-dried, and calcined for the XRD analysis.

Results and Discussion

Figure 1 schematically depicts the procedure developed for producing the cobalt oxide nanotubes. Briefly, alternate PDADMAC and PSS layers were first LbL assembled onto negatively charged PS particles (steps 1 and 2). The PE concentration (1 mg/mL) and the adsorption time (15 min) were chosen according to that reported in the literature[38] to afford saturated coverages onto the particle surfaces or the preceding PE layers. The comparison of the TEM image of the coated PS nanospheres with that of the uncoated ones (Figure 2) showed a PE shell thickness of 23 nm after 10 layers of PE adsorption. Such a value is consistent with values in previous studies.[38] The smooth surface of the PE-coated PS nanospheres suggests that the adsorption of 10 alternate PE layers was rather uniform.

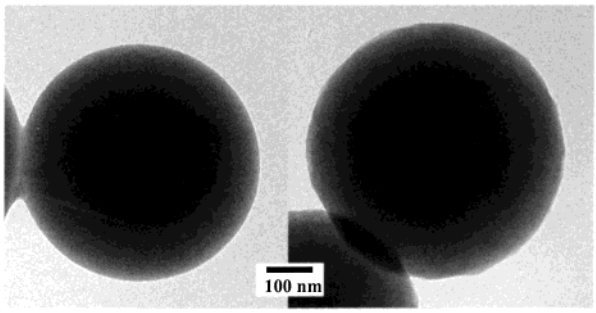

Figure 2. TEM images of 600 nm PS particles before (left) and after (right) coating of 10 PE multilayers.

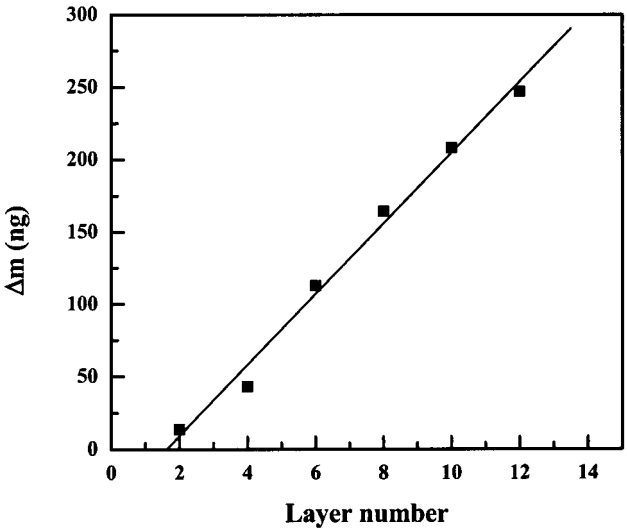

Figure 3. Relationship between the increase in mass of the Co(III)−cysteinato complex measured by a quartz crystal microbalance and the number of PE layers.

The infiltration of Co-S-cys into PE multilayer films precoated onto PS particles (step 3 in Figure 1) was verified by conducting similar experiments at a planar surface. Specifically, quartz crystals were employed as planar surfaces to form the PE deposition for the subsequent Co-S-cys infiltration. QCM is sensitive to the mass change[39,40] of a few subnanograms (also see eq 1) and should be suitable for following the mass increase due to the Co-S-cys infiltration into the PE multilayers. Figure 3 displays a linear relationship (R^2 = 0.99) between the mass increase (Δm) in the amount of Co-S-cys incorporation and the number of PE layers.

(37) Sauerbrey, G. Z. *Phys.* **1959**, *155*, 206.
(38) Caruso, F.; Lichtenfeld, H.; Donath, E.; Mohwald, H. *Macromolecules* **1999**, *32*, 2317−2328.
(39) Lu, C.; Czanderna, A. W. *Applications of Piezoelectric Quartz Crystal Microbalances*; Elsevier: Amsterdam, 1984; p 251.
(40) Ward, M. D.; Buttry, D. A. *Science* **1990**, *249*, 1000−1007.

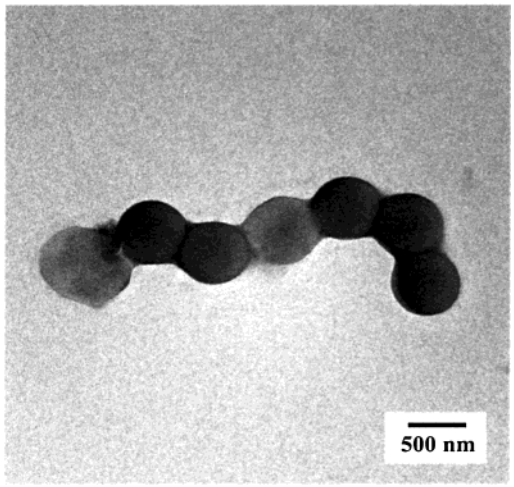

Figure 4. An TEM micrograph of a string of PS nanospheres covered with 10 PE layers containing the Co(III)−cysteinato complex.

Such a linear mass increase is indicative of the effective incorporation of the charged precursor into the PE assemblies of various volumes. The driving force for the precursor infiltration should be electrostatic interaction,[34] since no mass change was recorded when PDADMAC (whose charge is of the same polarity as that on the precursor) was the outermost layer. Evidently, the relationship shown in Figure 3 indicates that the amount of precursor infiltrated can be precisely controlled by varying the PE layer number, as recently demonstrated by Caruso and co-workers.[32]

Interestingly, the PE multilayer deposition onto the PS particles and the follow-up Co-S-cys infiltration led to the formation of a pearl necklace-like structure which is schematically shown in Figure 1. Figure 4 is a TEM image of the pearl necklace-like structure composed of seven interconnected nanospheres. It should be pointed out that only after the incorporation of the Co-S-cys precursor was formation of the pearl necklace-like composite particles observed. PS nanospheres coated with only the PE multilayers did not aggregate or interconnect. Note that the precursor, whose structure is shown in Figure 1, possesses functional groups for forming both intermolecular hydrogen and disulfide bonds. Utilizing other cobalt complexes as precursors (e.g., $[Co(bpy)_3]^+(ClO_4)^-$, bpy = bipyridine) which cannot form these types of bonds did not result in the production of the pearl necklace-like structures. To verify whether disulfide bonds are important, we attempted to use FTIR to detect the S−S stretching. Unfortunately, the spectrum of the sample is analogous to that of PE-coated PS particles. This similarity can be attributed to the fact that the precursor penetrated into the PE layers and was less abundant than the PS core particles and PE molecules. Consequently, the IR signals arising from the functional groups of the PS core particles and PE molecules overwhelmed that originated from the precursor. We therefore resorted to the choice of different precursors that contain functional groups for either hydrogen bonding or disulfide bond formation in an effort to investigate the chemical origin of the necklace-like structures. The driving force behind the threading of these as-prepared particles appears to be intermolecular hydrogen bonding, since use of cobalt complexes that are incapable of forming hydrogen bonds (but with or without the potential for the formation of disulfide bonds) only yielded broken hollow spheres.[41] This hypothesis is in line with some recent reports on the important role played by intermolecular hydrogen bonding in the construction of linear tubular peptide architecture,[42] organic calix[4]hydroquinone nanotubes,[43] and tubular silica structure from organogel template.[44] Another possibility is that particles containing the cobalt complex precursor could be interconnected by the nonisotropic interaction, which would induce the formation of Y-junction shaped structure.[45] The AFM image shown below appears to suggest this possibility.

Finally, the production of the cobalt-containing nanotubes was followed by TEM, SEM, and AFM, and the nanotubes were characterized by XRD, EDX, and HRTEM coupled with electron diffraction. Shown in parts A and B of Figure 5 are a TEM image and a HRTEM image, respectively. Both images clearly show that hollow cobalt-containing nanotubes had been produced. The inset of Figure 5A demonstrates that the electronic density of the tube edge (with a wall thickness of ca. 14 nm) is higher than that in the center of the tube. Note that the tube structure observed using regular TEM does not resemble the disordered carbon tubes on some commercial TEM grids. To further rule out this possible complication, we examined several TEM grids without any samples cast and found that the irregular carbon tubes (∼50−90 nm in diameter) are much smaller than the Co_3O_4 nanotubes (200−400 nm in diameter), and carbon tubes are rarely dispersed on the TEM grids. Fine tubular structures shown in the HRTEM image (Figure 5B) further indicate the production of Co_3O_4 nanotubes. Upon suspension in ethanol solution, the nanotubes had a dark brown color, suggesting that Co_3O_4 is probably the predominate structure.[46] The tube length and width were 3−4 μm and 200−400 nm, respectively. The length of 3−4 μm may arise from the fusion of 6−10 PS particles impregnated with the Co-S-cys precursor. The selected area electron diffraction pattern of a representative spot on the nanotube wall shown in Figure 5C depicts continuous rings, which are indicative of the cubic spinel Co_3O_4 structures (see the indexes of crystalline phases in Figure 5C). The rings are sharp and continuous, which suggests that the nanotubes consist of polycrystalline phases. The XRD pattern (Figure 6) again confirms that the nanotube composition is essentially of polycrystalline Co_3O_4 phase. No other phases (e.g., CoO) could be detected. The peaks at $2\theta = 30.2$, 37.9, 44.4, 59.5, 65.0 are indicative of the presence of the (220), (311), (400), (511), and (440) reflections of Co_3O_4.[47]

We have also observed cobalt oxide nanotubes at silicon substrates by SEM measurements.[41] From typi-

(41) Shi, X.; Han, S.; Sanedrin, R. J.; Galvez, C.; Ho, D. G.; Hernandez, B.; Zhou, F.; Selke, M. *Nano Lett.*, in press.
(42) Ghadiri, M. R.; Granja, J. R.; Milligan, R. A.; McRee, D. E.; Khazanovich, N. *Nature (London)* **1993**, *366*, 324−327.
(43) Hong, B. H.; Lee, J. Y.; Lee, C. W.; Kim, J. C.; Bae, S. C.; Kim, K. S. *J. Am. Chem. Soc.* **2001**, *123*, 10748−10749.
(44) Jung, J. H.; Shinkai, S.; Shimizu, T. *Nano Lett.* **2002**, *2*, 17−20.
(45) Tlusty, T.; Safran, S. A. *Science* **2000**, *290*, 1328−1331.
(46) Greenwood, N. N.; Earnshaw, A. *Chemistry of the Elements*, 4th ed.; Pergamon Press: Oxford, 1984; p 1297.
(47) Powder Diffraction File. *International Center for Diffraction Data*: Swarthmore, PA, 1991.

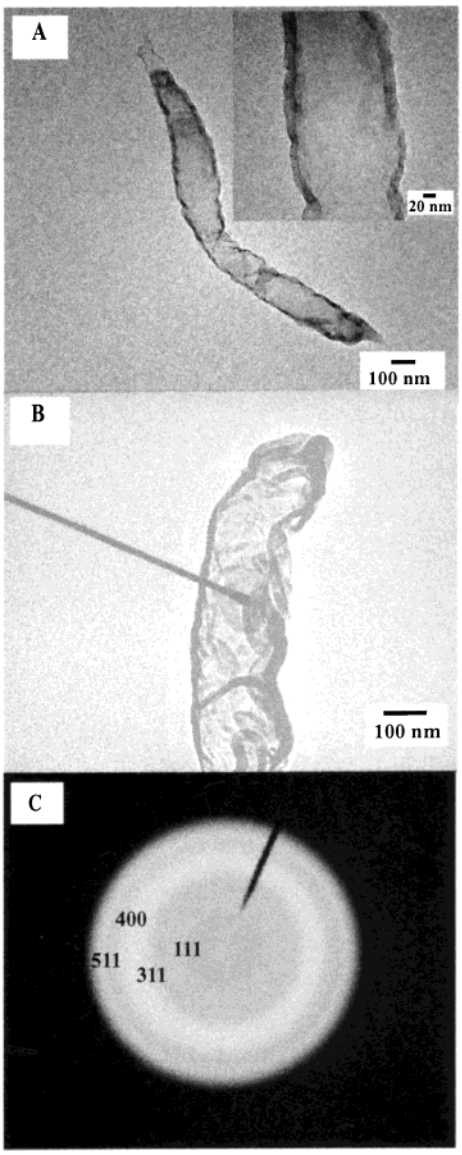

Figure 5. (A) A cobalt oxide nanotube produced by calcination of the pearl necklace-like structure consisting of the PE/precursor composite-coated particles (shown in Figure 4), (B) a high-resolution TEM image of a cobalt oxide nanotube, and (C) a selected area electron diffraction pattern of a representative spot on the same cobalt oxide nanotube, with characteristic indexes identified. The inset of (A) shows a higher magnification of the tube wall structure.

cal SEM images (50 × 40 μm), we found that 40% of the total Co_3O_4 products were present in nontubular structures. To ensure that the Co signal did not arise from the possible cobalt complex residue on silicon wafers, we deposited the nanotube suspension on silicon wafers and thoroughly washed with water prior to SEM measurements. An EDX analysis of the individual nanotubes in conjunction with SEM measurements indicates that the nanotubes contained Co (Figure 7), further confirming that the Co signal is associated with the nanotubes. C, N, and S were absent in the EDX spectrum, suggesting that the calcination step had effectively removed the PS core particles, PE multilayers, and the organic ligands of the precursor and converted the precursor into the final cobalt oxide nanotubes. Thus, it appears that the calcination step facilitated the reaction between Co and O_2 at an elevated temperature

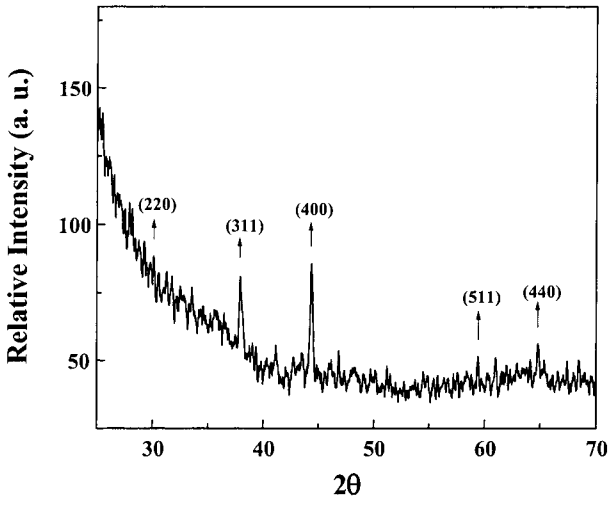

Figure 6. An XRD pattern of the Co_3O_4 nanotubes with the different phases identified.

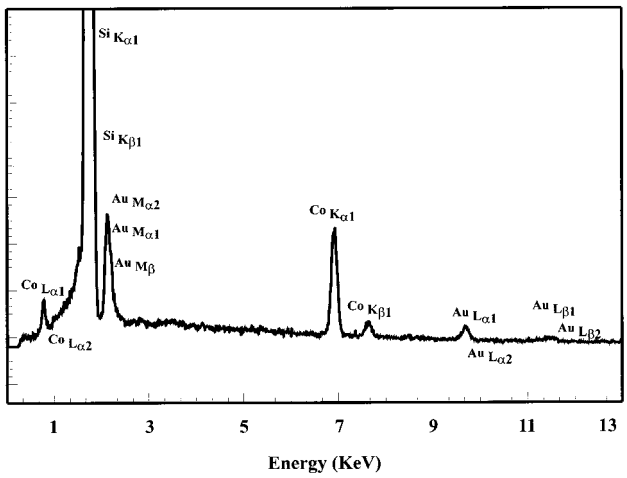

Figure 7. An EDX spectrum of a cobalt oxide nanotube, revealing the presence of cobalt. The presence of the gold signal is attributable to the thin Au film sputtered onto the structure for SEM imaging.

and eventually fused the oxidized Co present at the surfaces of the interconnected spheres to form nanotube structures.

We found that 10 layers of alternating PDADMAC and PSS layers onto PS particles were sufficient for the final formation of nanotubes after calcination. When the number of PE layers was less than 6, no nanotubes were obtained. This implies that the formation of the nanotubes is highly dependent on the amount of the precursor loaded into the PE multilayered shell. Another important preparative parameter is the calcination time. With an insufficient calcination time (e.g., N_2 for 2 h and O_2 for 2 h), only fractured tubes were obtained (Figure 8A). When nanotubes were produced under the optimized preparative conditions, multiple cobalt oxide nanotubes with relatively uniform diameters could be easily observed by AFM (Figure 8B).

Conclusion

Cobalt oxide nanotubes were created using a colloidal templating approach. A variety of surface and elemental analysis techniques (TEM, SEM, AFM, XRD, electron diffraction, and EDX) were employed to char-

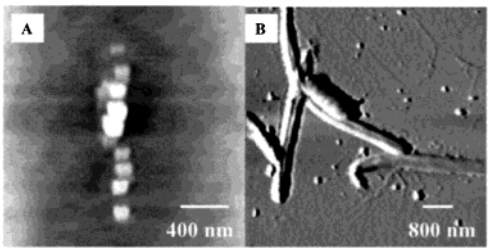

Figure 8. AFM images of (A) a fractured nanotube formed from a 4 h calcination (2 h under N_2 and 2 h under O_2) and (B) multiple cobalt nanotubes formed after an 8 h calcination.

acterize the structure and the chemical composition of the nanotubes. These nanotubes were found to be composed of spinel polycrystalline Co_3O_4. The length and width of these tubes, with a wall thickness of ca. 14 nm, were 3−4 μm and 200−400 nm, respectively. The preparative parameters (e.g., precursor infiltration time, PE layer number, and calcination time) were also investigated and optimized. The metal complex Co-S-cys used in this study is probably the critical factor for the tube formation, as cobalt complexes that do not possess sites for H-bonding did not produce the tubes. The preparation of such cobalt oxide nanotubes via the procedure outlined in this work represents a new route for constructing metal-containing nanotubes through the combination of colloidal templating, layer-by-layer polyelectrolyte deposition, and a judicious choice of the metal-containing precursor. Experiments to evaluate the exact reason for the formation of these strings of nanospheres will be reported elsewhere.

Acknowledgment. We thank Julia Pilloni and Jiaxing Huang (University of California, Los Angeles) for their assistance with the TEM and SEM measurements and William Wimberley (CSULA) for his help with the TEM image processing. We are also grateful to the three anonymous reviewers for their constructive comments about our data interpretation. Financial support from the NIH-SCORE subprojects (GM 08101 for F.Z. and M.S.), the NSF-CRUI grant (DBI-9978806 for F.Z.), and a NIH-AREA grant (GM 63530-01 for F.Z.) is gratefully acknowledged.

CM011630I